

Effect of Kaolin on the Thermal Conversion Performance of Zhundong Sub-bituminous Coal

Nan Xiao, Xiaobo Hu, Wenlong Mo,* Guanjun Jing, Xing Fan, Xiaoqin Yang, Shupeizhang, and Xianyong Wei

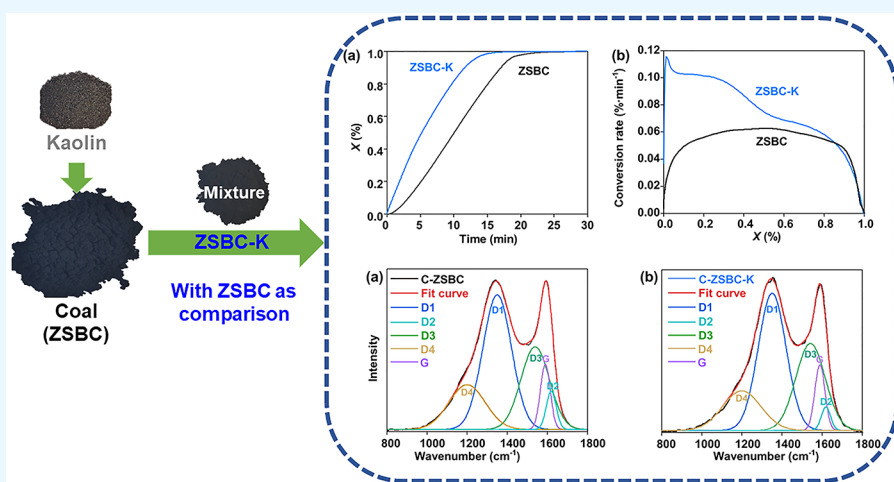
Cite This: *ACS Omega* 2023, 8, 30129–30138

Read Online

ACCESS |

Metrics & More

Article Recommendations



ABSTRACT: In order to investigate how kaolin affects the structure and thermal conversion performance of Zhundong sub-bituminous coal (ZSBC), this study focused on analyzing the pyrolysis, combustion, and gasification of both ZSBC and a mixture of kaolin and Zhundong sub-bituminous coal (ZSBC-K) using the TG-DTG technique. The findings demonstrated that the addition of kaolin enhanced the pyrolysis and combustion performance of ZSBC-K. To explain the above phenomena, the composition and structure of char from ZSBC and ZSBC-K were characterized by Fourier transform infrared spectroscopy (FTIR), X-ray diffraction (XRD), Raman spectroscopy (Raman), scanning electron microscopy (SEM) and X-ray photoelectron spectroscopy (XPS). The results showed that the addition of kaolin decreased the degree of graphitization of char and increased the relative content of oxygen on the surface of the char. Moreover, the addition of kaolin increased the degree of disorder of the char and formed more char pores. The rich pores were conducive to the entry of the gasification agent into the coal char particles, which enhanced the gasification activity. Additionally, the coal char mixed with kaolin contains several oxygen-containing functional groups and defect sites that facilitate the cracking and gasification performance of the macromolecular network's aromatic ring structure.

1. INTRODUCTION

Xinjiang Zhundong sub-bituminous coal (ZSBC), with a high volatile content, low ash content, and high calorific value, can be used as a raw material for pyrolysis, combustion, and gasification.^{1,2} However, ZSBC contains a large amount of alkali metals such as Ca, Na, and K and alkaline earth metals (AAEMs). The volatilization of AAEMs might cause serious slagging in industrial thermal conversion equipment.³ Research showed that the combination of coal or additives rich in silicon and aluminum with ZSBC can alleviate scaling and slagging problems.⁴ Zhu et al.⁵ compared the effect of silica–aluminum base additives such as kaolin, alumina, quartz sand, and found that kaolin presented a better antisludging effect. Therefore, the use of kaolin as an additive to improve slagging resistance

during high-temperature coal thermal conversion processes has gained widespread attention.

Zhang et al.⁶ found that the nonflammable inorganic minerals, such as SiO_2 and Al_2O_3 , present in kaolin could diminish the combustion performance of ZSBC. However, Wornat^{7,8} et al. used proton magnetic resonance thermal

Received: April 14, 2023

Accepted: July 11, 2023

Published: August 8, 2023



Table 1. Industrial Analysis and Elemental Analysis of Samples (wt %)^a

sample	proximate analysis (ad)				ultimate analysis (daf)				
	M_{ad}	A_{ad}	V_{ad}	FC_{ad}	C	H	O ^{diff}	N	S
ZSBC	10.96	2.40	28.34	58.31	68.42	4.27	24.20	2.63	0.48
ZSBC-K	10.72	11.09	25.54	53.65					

^aAbbreviations: ad, air-dry basis; M_{ad} , moisture; A_{ad} , ash; V_{ad} , volatiles; FC, fixed carbon; daf, dry and ash-free basis; diff, by difference.

Table 2. Ash Composition of ZSBC and ZSBC-K (wt %)

sample	CaO	Fe ₂ O ₃	SO ₃	MgO	Na ₂ O	Al ₂ O ₃	SiO ₂	SrO	Cl	K ₂ O	B ^a
ZSBC	47.97	20.45	11.37	5.32	4.39	2.65	2.56	1.89	1.80	0.10	15.0153
ZSBC-K	43.01	19.99	10.94	4.46	3.56	4.27	8.03	1.69	1.70	0.49	5.8138

^aB = (Fe₂O₃ + CaO + MgO + Na₂O + K₂O)/(SiO₂ + Al₂O₃).

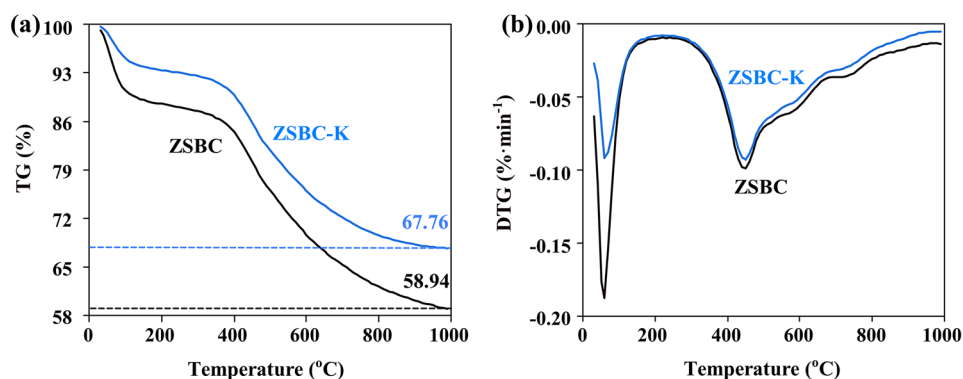


Figure 1. (a) TG curves of ZSBC and ZSBC-K with N₂ as the carrier gas. (b) DTG curves of ZSBC and ZSBC-K with N₂ as the carrier gas.

analysis and found that ion-exchanged AAEMs in coal could inhibit the pyrolysis process. The addition of kaolin, on the other hand, was shown to increase the pyrolysis activity of coal. Xu et al.^{9–11} conducted acid washing on coal and discovered that AAEMs had a significant catalytic effect on coal pyrolysis, while the addition of kaolin reduced coal pyrolysis reactivity. Furthermore, Xu et al.⁹ argued that the loss of AAEMs during gasification would weaken their catalytic effect. Additionally, adding kaolin might decrease the active sites of coal char, leading to a decline in gasification performance.¹² To analyze the impact of kaolin on the gasification process of ZSBC, it is essential to examine the changes in the composition and structure of coal char resulting from the addition of kaolin. Additionally, it would be valuable to further investigate the gasification mechanism of kaolin and its influence on coal.

For this study, Zhundong sub-bituminous coal and a mixture of Zhundong sub-bituminous coal with kaolin were examined. The TG-DTG technique was utilized to assess the samples' pyrolysis, combustion, and gasification performance under the condition of N₂, air, and CO₂, respectively. Fourier transform infrared spectroscopy (FTIR), X-ray diffraction (XRD), Raman spectroscopy (Raman), scanning electron microscopy (SEM) and X-ray photoelectron spectroscopy (XPS) were used to analyze the functional groups, crystal structure, microscopic morphology, and chemical bond composition of samples.

2. MATERIALS AND METHODS

2.1. Sample Preparation. Zhundong sub-bituminous coal (ZSBC) was acquired from the Wucuiwan (WCW) mine area Zhundong, Xinjiang, China. Prior to experimentation, the coal was crushed with a pulverizer and sifted to achieve a particle

size of less than 74 μm. Additionally, mechanically mixed kaolin with ZSBC in a mass ratio of 1:9 was labeled as ZSBC-K. To conduct an industrial analysis and element analysis of ZSBC and ZSBC-K, GB/T 212-2008 and GB/T 30732-2014 standards were followed.

2.2. Thermal Conversion Experiments. Thermogravimetric analyzer (SDTQ600 TA Instruments, USA) was used to test the pyrolysis and combustion characteristics of the samples in N₂ and oxidizing atmospheres, respectively, from room temperature to 1000 °C at a heating rate of 5 °C/min. Additionally, the same equipment was used to heat the samples from room temperature to 900 °C at a heating rate of 20 °C/min under a N₂ atmosphere. After stabilizing for 10 min, the gas was switched to a CO₂ atmosphere and reacted for 30 min to test the gasification reactivity of the samples.

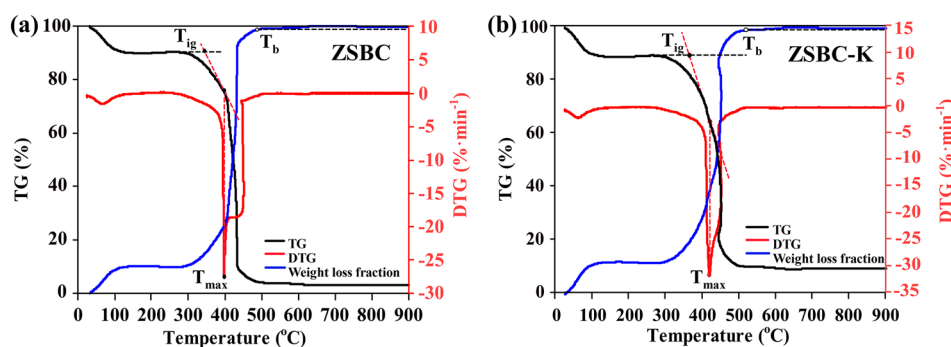
2.3. Char Preparation. Both ZSBC and ZSBC-K were placed separately in a tubular furnace, and N₂ was used as the carrier gas. The pyrolysis was carried out at a gas velocity of 60 mL/min. The reactor was heated from room temperature to 900 °C at a heating rate of 20 °C/min to investigate the thermal behavior of the samples during pyrolysis. After reaching 900 °C, the samples were held at that temperature for 30 min before being cooled to room temperature to obtain char. The resulting chars were named C-ZSBC and C-ZSBC-K, respectively, and were further analyzed for their physical and chemical properties.

2.4. Characterization Test. The types of functional group structure of the samples were analyzed by an infrared spectrometer (EQUINOX-55, Bruker, Germany). The microstructures of the carbonaceous components in each sample were analyzed using a Raman spectrometer (SENTERRA, Bruker, Germany), with three points selected from each

Table 3. Characteristic Pyrolysis Parameters of ZSBC and ZSBC-K

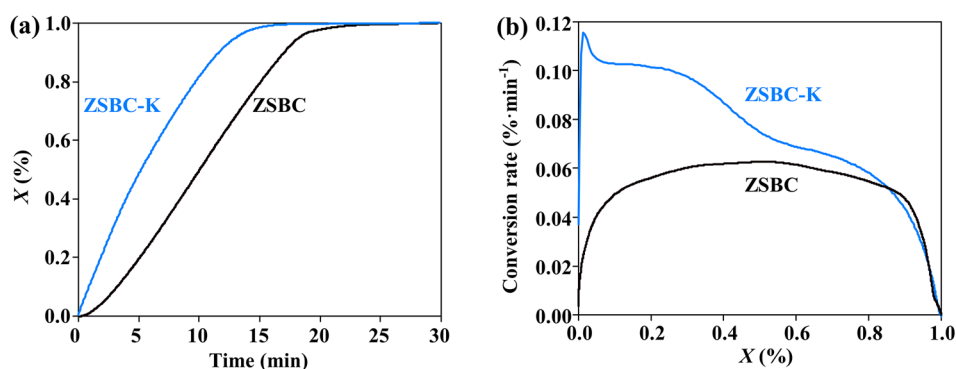
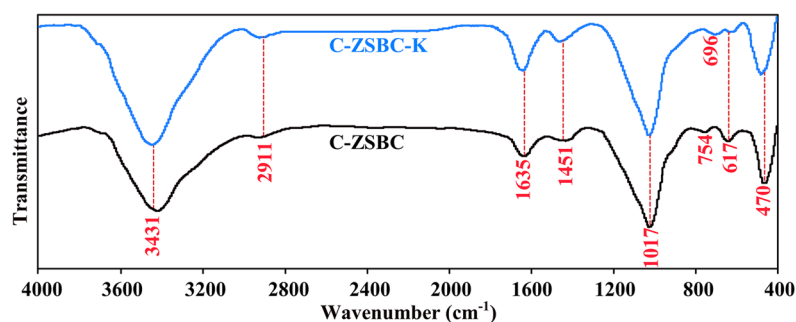
coal sample	T_s (°C)	T_f (°C)	T_{max} (°C)	$\Delta T_{1/2}$ (°C)	$(dw/dt)_{max}$ (% s)	$(dw/dt)_{mean}$ (% s)	D ($10^{-10} \%^2 \text{ } ^\circ\text{C}^{-3} \text{ s}^{-2}$) ^a
ZSBC	239	659	449	235	-0.0988	-0.0390	1.53
ZSBC-K	220	680	450	231	-0.0926	-0.0334	1.35

$$^a D = [(dw/dt)_{max} \cdot (dw/dt)_{mean}] / (T_{max} \cdot T_s \cdot \Delta T_{1/2}).$$

**Figure 2.** (a) TG curves of ZSBC with air as the carrier gas. (b) DTG curves of ZSBC-K with air as the carrier gas.**Table 4. Characteristic Combustion Parameters of ZSBC and ZSBC-K**

coal sample	T_{ig} (°C)	T_b (°C)	T_{max} (°C)	$(dw/dt)_{max}$ (% s)	$(dw/dt)_{mean}$ (% s)	S ($10^{-7} \text{ s}^{-2} \text{ } ^\circ\text{C}^{-3}$) ^a
ZSBC	343	473	397	-27.49	-1.099	5.398
ZSBC-K	373	488	418	-31.36	-1.027	4.743

$$^a S = [(dw/dt)_{max} \cdot (dw/dt)_{mean}] / T_{ig}^2 \cdot T_b.$$

**Figure 3.** (a) Carbon conversion versus time of ZSBC and ZSBC-K. (b) Reaction rate versus carbon conversion of ZSBC and ZSBC-K.**Figure 4.** FTIRS spectra of C-ZSBC and C-ZSBC-K.

sample for spot analysis. The composition and chemical valence of surface elements were measured by X-ray photoelectron spectroscopy (ULVAC PHI 5000 Versa Probe-II, PerkinElmer, America), The binding energy of the O element was corrected using the C 1s peak at 284.6 eV as a reference point. The surface microstructure of each sample was observed

using a scanning electron microscope (MIRA4, TESCAN, Germany).

3. RESULTS AND DISCUSSION

3.1. Proximate and Ultimate Analyses. The results of this analysis are presented in Table 1. As shown in Table 1,

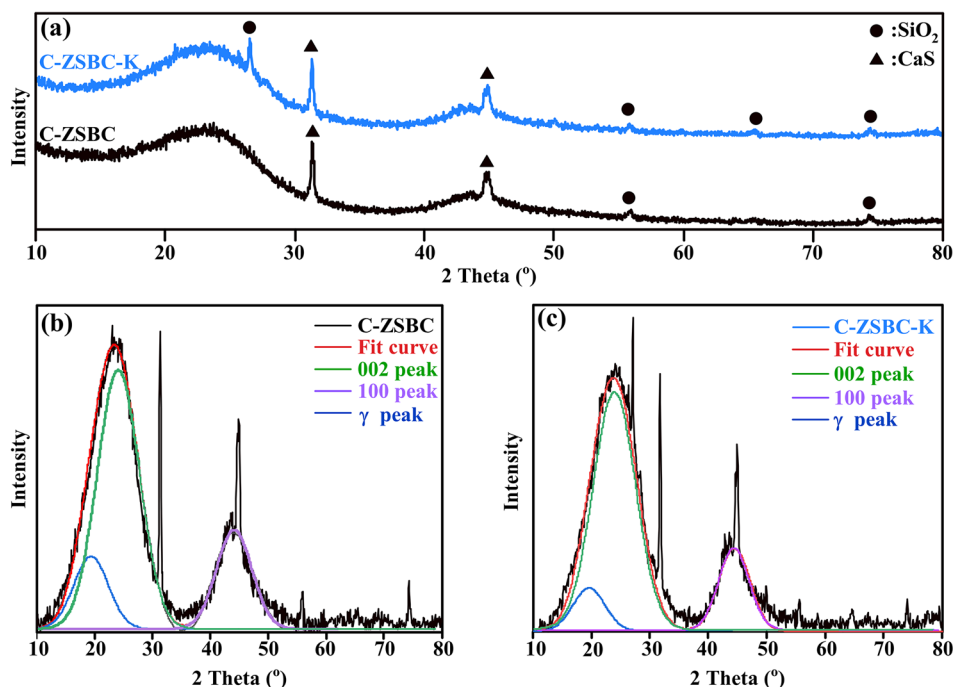


Figure 5. (a) XRD patterns of ZSBC and ZSBC-K. (b) Fitting curves of the XRD pattern of C-ZSBC. (c) Fitting curves of the XRD pattern of C-ZSBC-K.

Table 5. Structural Parameters of C-ZSBC and C-ZSBC-K X-ray Diffraction

sample	$2\theta_{002}$ (deg)	$\text{fwhm}_{(002)}$ (deg)	$2\theta_{100}$ (deg)	$\text{fwhm}_{(100)}$ (deg)	d_{002} (nm)	L_c (nm)	L_a (nm)
C-ZSBC	24.048	8.619	44.515	7.398	0.370	6.03	14.04
C-ZSBC-K	23.965	8.733	44.280	6.285	0.371	5.63	16.37

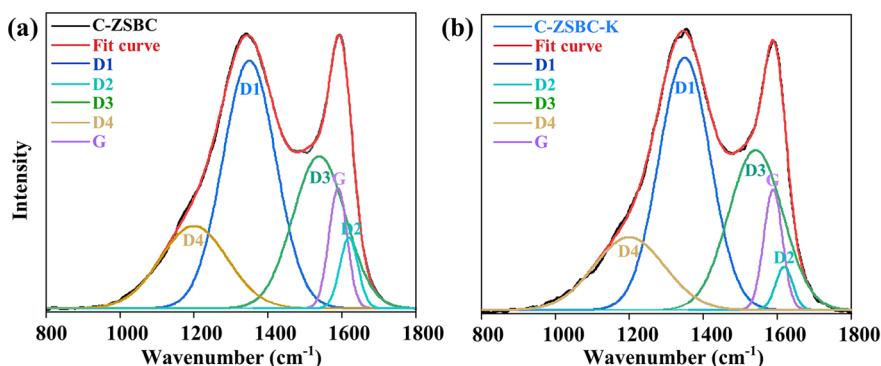


Figure 6. (a) Raman spectrum fitting curves of C-ZSBC. (b) Raman spectrum fitting curves of C-ZSBC-K.

ZSBC has a low ash content of only 2.40% and its volatile content is less than 30%. Furthermore, its fixed carbon content is high, approaching 60%. Therefore, ZSBC can serve as a viable raw material for coal gasification.

3.2. Ash Composition Analyses. Table 2 shows the ash composition analysis of ZSBC and ZSBC-K. A comparison between the two reveals that the ash obtained from ZSBC-K has a lower content of sodium, calcium, and magnesium compared to ZSBC. Conversely, the content of silicon and aluminum in the ash of ZSBC-K is higher. Hence, it can be inferred that the addition of kaolin reduces the proportion of AAEMs in ZSBC. By calculation of the alkalinity index (B value) of the two coal ashes, it was found that the B value of ZSBC-K was reduced by 67% compared with ZSBC,

demonstrating that the alkalinity of ZSBC ash decreased significantly with the addition of kaolin.

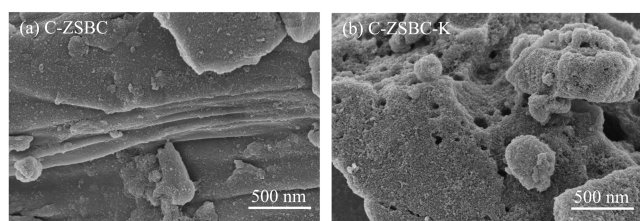
3.3. Thermochemical Conversion. **3.3.1. Thermal Weight Loss Characteristic Analysis (N_2 Atmosphere).** Figure 1 displays the thermogravimetric curves for ZSBC and ZSBC-K. As illustrated in Figure 1a, ZSBC experiences a weight loss of 41.06%, whereas ZSBC-K only loses 32.24%. This suggests that ZSBC has a higher concentration of volatile substances. Additionally, Figure 1b shows that the pyrolysis of samples has four main stages.¹³ The first stage is from 40 to 240 °C. It corresponds to dehydration and degassing, while the second stage involves the initial pyrolysis, taking place from 240 to 350 °C, during which weak bonds^{14,15} in the coal macromolecular network structure break down, generating small molecular gas.

Table 6. Assignment and Area of Raman Spectrum Fitting Peaks of C-ZSBC and C-ZSBC-K

band	center (cm ⁻¹)	assignment	area percentage (%)	
			C-ZSBC	C-ZSBC-K
G	1580	stretching vibration mode of carbon atom in the graphite crystal	7.25	7.55
D1	1350	vibration of disordered graphitic lattices within plan imperfections, such as defects and heteroatoms	43.57	43.62
D2	1620	vibration mode involving graphene layers	4.26	2.48
D3	1530	amorphous sp ² -band forms, including organic molecules, fragments, or functional groups, and in poorly organized carbonaceous materials	26.66	29.15
D4	1200	mixed sp ² -sp ³ mixed bond in poorly organized structures, such as the periphery of crystallites	18.26	17.20

Table 7. Raman Band Area Ratio of C-ZSBC and C-ZSBC-K

sample	I _{D1} /I _G	I _{D3} /I _G	I _{D3} /I _{G+D2+D3}	I _{D3} /I _{D1}	I _{D3} /I _{All}
C-ZSBC	6.009	3.669	0.698	0.612	26.66
C-ZSBC-K	5.777	3.861	0.774	0.668	29.15

**Figure 7. (a) SEM image of C-ZSBC. (b) SEM image of C-ZSBC-K.**

Meanwhile, the functional group mainly composed of carboxyl groups decomposes into gas components. At this stage, the weight loss is minimal. The third stage is the main pyrolysis stage, occurring between 350 and 700 °C. During this phase, the coal matrix undergoes extensive depolymerization and decomposition reactions, resulting in the production of large-molecule volatile matter and char. The fourth stage is the secondary degassing stage that occurs above 700 °C. During this stage, polycondensation reactions occur in the char, resulting in the production of gases and a small amount of tar. There is also a possibility that the char undergoes continuous aromatization.¹⁴ Observing the DTG curve in Figure 1b, we can see that in the first stage, the dehydration and degassing peak of ZSBC-K are lower and narrower, which is consistent with the relatively low moisture content of ZSBC-K found in the ultimate analysis in Table 1. In the second stage, the curves of ZSBC and ZSBC-K are similar, but the weight loss of ZSBC is slightly higher. In the third stage, the weight loss of ZSBC is relatively high, which may be related to the possibility that the AAEMs in ZSBC increase the pyrolysis activity. In the fourth stage, the weight loss of ZSBC-K is relatively lower. This could be because kaolin promotes the enlargement of aromatic nuclei while inhibiting the release of some small molecules.¹³

In order to quantitatively describe the difference between ZSBC and ZSBC-K in the thermogravimetric process, several characteristic points are selected from the DTG curve in Figure 1b to characterize the thermogravimetric behavior,^{16,17} including T_s (initial volatile release temperature), $(dw/dt)_{\max}$ (maximum volatile release rate), T_{\max} (temperature corre-

sponding to the maximum volatile release rate), T_f (temperature at the end of the main pyrolysis stage), and $\Delta T_{1/2}$ (temperature range of $(dw/dt)/(dw/dt)_{\max} = 1/2$); the results are shown in Table 3. Generally, the smaller T_{\max} and larger absolute values of $(dw/dt)_{\max}$ and $(dw/dt)_{\text{mean}}$ indicate stronger volatile emission. Comparing ZSBC with ZSBC-K, it is observed that the absolute values of $(dw/dt)_{\max}$ and $(dw/dt)_{\text{mean}}$ are lower in ZSBC-K and T_{\max} is higher, demonstrating a lower release intensity of volatiles in ZSBC-K. To summarize the effects of the aforementioned characteristic parameters on volatilization release behavior, the comprehensive devolatilization index D^{13} is introduced. A higher D value indicates a faster release of volatiles and greater pyrolysis activity. From Table 3, it can be observed that the D value of ZSBC-K is lower than that of ZSBC, which further indicates that ZSBC-K has lower pyrolysis reactivity. This implies that the mechanically mixed ZSBC-K does not promote the pyrolysis reactivity of coal samples but rather inhibits it.

3.3.2. Combustion Characteristics. Figure 2 displays the combustion curves of both ZSBC and ZSBC-K. It is clear from the figure that ZSBC has a weight loss of 96.63%, while ZSBC-K has a weight loss of 90.01%. The presence of non-combustible inorganic minerals such as SiO₂ and Al₂O₃ in kaolin⁶ causes the weight loss of ZSBC-K to be smaller compared to ZSBC. During the low-temperature stage (<100 °C), ZSBC and ZSBC-K experience a gradual decrease in weight due to the removal of moisture in coal. However, at 300–600 °C, because of the intense combustion of volatile and fixed carbon in samples, the weights of ZSBC and ZSBC-K decrease significantly, and the rate of weight loss shows a significant peak. Upon comparing the DTG curves of both ZSBC and ZSBC-K, it becomes apparent that the addition of kaolin causes the DTG curve of ZSBC to shift toward a higher temperature zone. Further research shows that the AAEMs present in coal can act as catalysts during combustion.^{18,19} However, the addition of kaolin reduces the amount of alkali metals in ZSBC, which in turn decreases the catalytic effect and increases the activation energy required for combustion. This results in a shift of the DTG curve of ZSBC toward a higher temperature zone and a reduction in its combustion performance, as demonstrated by research.^{20,21}

To comprehend the combustion behavior of ZSBC and ZSBC-K, the TG/DTG tangent method is utilized to evaluate the coal's combustion characteristic temperatures,²² comprising T_{ig} (ignition temperature), T_{\max} (peak temperature), and T_b (burnout temperature) as illustrated in Figure 2 and Table 4. It can be observed from Table 4 that the T_{ig} value of ZSBC-K is 30 °C higher than that of ZSBC, suggesting that the burnout time of ZSBC-K is longer. Additionally, the T_b and T_{\max} values of ZSBC-K are higher than those of ZSBC, indicating that the combustion activity of ZSBC-K is lower than that of ZSBC. In order to further study the combustion characteristics of coal samples, the comprehensive combustibility index (S) reflects the burning ability of fuels,^{21,23} and the higher the value of S , the higher the combustion reactivity will be. These parameters could be calculated by the equation

$$S = (dw/dt)_{\max} (dw/dt)_{\text{mean}} / T_i^2 T_b$$

The results of S are shown in Table 4. The S value of ZSBC-K is higher than that of ZSBC, possibly because ZSBC-K contains less volatile matter and more ash content (11.09%). A higher ash content can easily agglomerate, which increases heat and mass transfer resistance, inhibiting combustion.²⁴ The

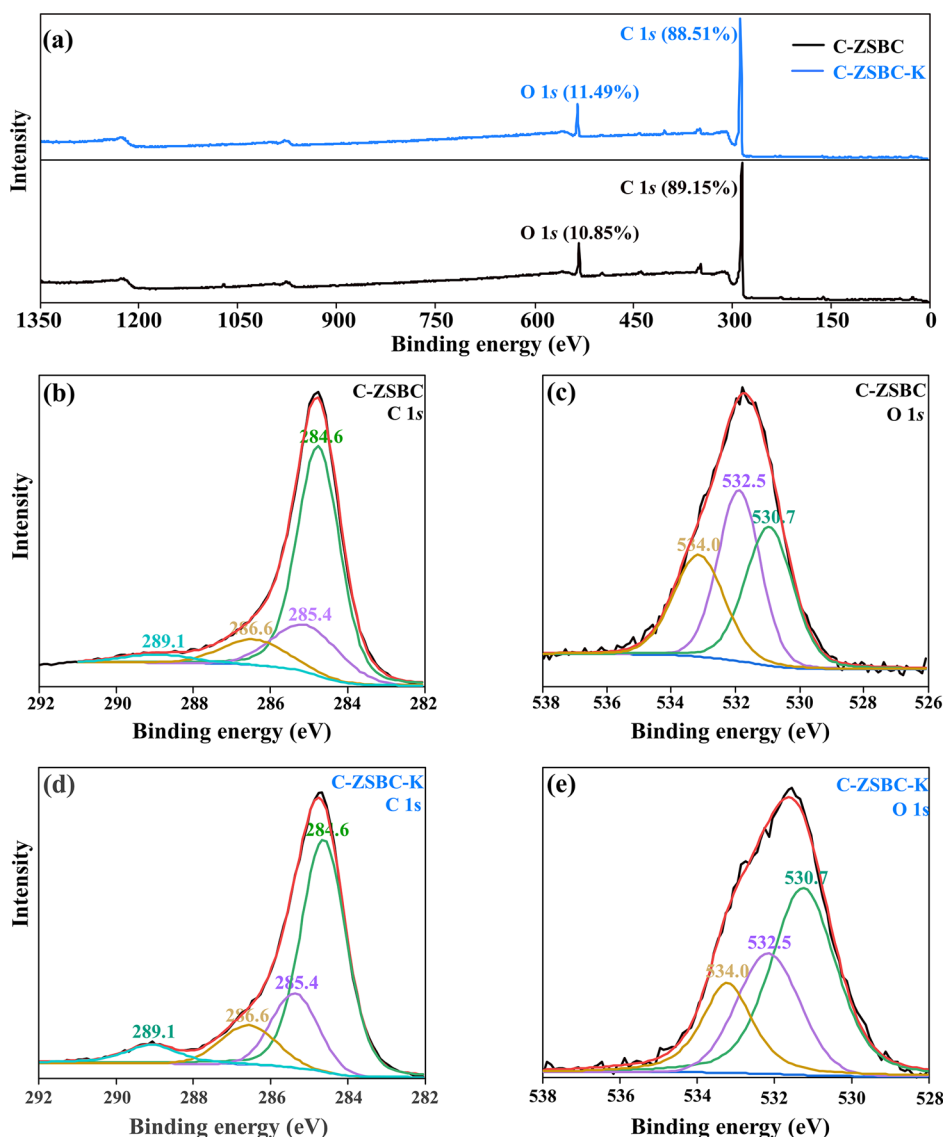


Figure 8. (a) XPS survey spectra of the coal samples. (b) XPS C 1s spectrum of C-ZSBC. (c) XPS O 1s spectrum of C-ZSBC. (d) XPS C 1s spectrum of C-ZSBC-K. (e) XPS O 1s spectrum of C-ZSBC-K.

Table 8. Distribution of C and O Forms in C-ZSBC and C-ZSBC-K from Analysis with XPS

elemental peak	functionality	binding energy (eV)	molar content (%)	
			C-ZSBC	C-ZSBC-K
C 1s	>C-C</td> <td>284.6</td> <td>65.84</td> <td>57.35</td>	284.6	65.84	57.35
	>C-H	285.4	19.11	23.89
	>C=O	286.6	11.27	11.39
	-COOH	289.1	3.78	7.38
O 1s	>C=O	530.7	35.31	54.75
	>C-O-	532.5	37.22	26.95
	COO ⁻	534.0	27.47	18.30

results show that the combustion performance of ZSBC becomes worse after adding kaolin.

3.3.3. Analysis of Gasification Characteristics (CO₂ Atmosphere). Figure 3 depicts the relationship between the carbon conversion rate and the time of the CO₂ gasification for

ZSBC and ZSBC-K, as well as the relationship between the gasification rate and the carbon conversion rate. The gasification time of ZSBC-K is shorter than that of ZSBC, and for carbon conversion rates below $X < 0.85$, the gasification rate of ZSBC-K is much higher, indicating a higher gasification activity for this material. For both samples, when the conversion rate exceeds 0.85, their gasification rates are significantly reduced. This is due to the gradual reduction of organic matter, particularly the carbonaceous component, and the gradual increase in ash content during gasification.^{24–26}

The reactivity index $R_{0.5}$, defined as $0.5/t_{0.5}$, where $t_{0.5}$ represents the gasification time (min) when the conversion rate reaches 50%, is used to quantitatively evaluate the gasification reactivity of ZSBC and ZSBC-K.^{27,28} The results indicate that ZSBC-K has a higher gasification reactivity than ZSBC, with $R_{0.5}$ values of 0.094 and 0.050, respectively. This means that the gasification reactivity of ZSBC-K is roughly twice that of ZSBC. To provide an explanation for the observed phenomenon,²⁸ the composition and structure of

ZSBC and ZSBC-K char are further characterized in order to study the changes in composition and carbon structure of coal char during gasification. Various analytical techniques are employed to characterize the composition and structure of the char samples in detail.

3.4. Char Structure Characterization. **3.4.1. FTIR Analysis.** The FTIR analysis results are shown in Figure 4. The absorption peaks of C-ZSBC and C-ZSBC-K at 3431 cm^{-1} are assigned to OH stretching vibration. These hydroxyl groups are derived from hydrated minerals or H_2O molecules present in the char.^{29,30} The strength and area of the peak for C-ZSBC-K at this position are higher than those of C-ZSBC. This could be attributed to the presence of hydrated minerals such as kaolinite in kaolin, which results in the formation of more hydroxyl groups in C-ZSBC-K due to the loss of crystal water during high-temperature pyrolysis.³¹ The absorption peaks at 2920 and 1451 cm^{-1} correspond to the antisymmetric stretching of n-CH_2 and asymmetric angular vibration of $-\text{CH}_3$,³² respectively. The peak strength of C-ZSBC-K at these positions is higher than that of C-ZSBC. Li stated that $-\text{CH}_x$ can promote the high-temperature thermochemical reaction of substances,³³ which is consistent with the experimental results that the gasification performance of C-ZSBC is enhanced after adding kaolin. The absorption peaks at 1635 and 1017 cm^{-1} are attributed to the stretching vibration of $\text{C}=\text{O}$ and the stretching vibration of $\text{C}-\text{O}-\text{C}$ in aromatics,³⁴ respectively. The peak intensity of C-ZSBC-K at these two places is higher than that of C-ZSBC, indicating that the addition of kaolin deepens the aromatization degree of C-ZSBC.²³ The absorption peaks at 754 and 696 cm^{-1} in C-ZSBC and C-ZSBC-K respectively correspond to the $\text{Si}-\text{O}-\text{Si}$ symmetric tensile vibration of quartz.³⁵ The absorption peak at 470 cm^{-1} is attributed to kaolinite, resulting from the asymmetric expansion of $\text{Si}-\text{O}-\text{Al}$ and the bending vibration of $\text{O}-\text{Si}-\text{O}$.³⁵ Since kaolin mainly consists of kaolinite,³⁶ the stronger peak intensity observed in C-ZSBC-K compared to C-ZSBC suggests a higher kaolin content in C-ZSBC-K.

3.4.2. XRD Analysis. The XRD spectra of both C-ZSBC and C-ZSBC-K are shown in Figure 5a. It has been found that CaS and SiO_2 coexist in both materials.¹² However, C-ZSBC-K exhibits more pronounced SiO_2 characteristic peaks, which can be attributed to the addition of kaolin. This addition has been known to increase the SiO_2 content in C-ZSBC as reported in previous studies. Moreover, Figure 5a shows two peaks that can characterize the microcrystalline structure of the material: the (002) peak, which represents the degree of orientation of macromolecules in the aromatic plane at $22\text{--}24^\circ$, and the (100) peak, which represents the size of the aromatic plane at 44° .^{36,37} Following the addition of kaolin, the intensity of the (002) peak in C-ZSBC decreases. This suggests that the addition of kaolin disrupts the directional arrangement of aromatic plane macromolecules, leading to an increase in the degree of disorder.³⁸ To further analyze the changes in the microcrystalline structure of C-ZSBC after the addition of kaolin, the XRD curve was fitted with peaks, and the results are presented in Figure 5b,c. Notably, the γ peak appears on the left side of the (002) peak. This peak is the aliphatic side chain connected by the edge of the microcrystal, which results in the asymmetry of the (002) peak.^{36,37}

The microcrystalline structure parameters of both C-ZSBC and C-ZSBC-K are calculated using the Bragg equation and Scherrer formula.³⁷ Table 5 presents the calculated microcrystalline structure parameters where d_{002} represents the

interlayer spacing, L_c refers to the stacking height of the layer, and L_a represents the diameter of the layer. Interestingly, following the addition of kaolin, there is an increase in the L_a value of C-ZSBC, while the L_c value decreases. This phenomenon is thought to be caused by polycondensation inside the coal char, dehydrogenation of hydrogenated aromatics, and cracking of heterocycles leading to the generation of more aromatic ring structures.³⁷ The decrease in vertical stacking height could be attributed to the thinner lamellar structure that is easier to move, thus facilitating the graphitization process during gasification.³⁹ The addition of kaolin to C-ZSBC results in a decrease in the stacking thickness of microcrystals, an increase in the space between microcrystals, an increase in defects, and a more disordered graphite structure within C-ZSBC.³⁸ These changes indicate that the addition of kaolin inhibits the graphitization tendency of C-ZSBC and improves its gasification activity.

3.4.3. Raman Analysis. Figure 6 illustrates the Raman spectra of C-ZSBC and C-ZSBC-K along with their respective fitting peaks, which are presented in Table 6. Based on the spectrum, it can be observed that the D1, G, and D3 peaks in C-ZSBC-K are stronger compared to C-ZSBC, while the D2 band is weaker. These findings suggest that the carbon crystal structure in C-ZSBC-K is more disordered than that in C-ZSBC.^{40,27,12}

To better characterize the structural changes of char, the area ratio of the Raman band is introduced as a semi-quantitative parameter, which is presented in Table 7.³¹ The $I_{\text{D1}}/I_{\text{G}}$ and $I_{\text{D3}}/I_{\text{G}}$ ratios represent the degree of graphitization and the order of the samples. A higher $I_{\text{D1}}/I_{\text{G}}$ value or a lower $I_{\text{D3}}/I_{\text{G}}$ value indicates a lower degree of carbon structure order. The $I_{\text{D1}}/I_{\text{G}}$ ratio of C-ZSBC-K is higher, while the $I_{\text{D3}}/I_{\text{G}}$ ratio is lower. This suggests that the addition of kaolin inhibits the graphitization process of C-ZSBC-K and increases the degree of char disorder. Moreover, the $I_{\text{D3}}/I_{\text{G+D2+D3}}$ value reveals the content of amorphous carbon structure in coal char.⁴¹ Compared to C-ZSBC-K, the $I_{\text{D3}}/I_{\text{G+D2+D3}}$ value of C-ZSBC-K is higher, indicating a greater presence of an amorphous carbon structure. The $I_{\text{D3}}/I_{\text{D1}}$ ratio characterizes the ratio of small-ring aromatic structures to dense-ring aromatic structures, and the $I_{\text{D3}}/I_{\text{D1}}$ ratio of C-ZSBC-K is relatively large. It can be inferred that the addition of kaolin destroys the microcrystalline or dense ring structure in C-ZSBC and converts it into a structure with more defects and amorphous carbon, characterized by small-ring aromatic structures. Additionally, $I_{\text{D3}}/I_{\text{All}}$ indicates the number of reactive active sites.⁴² The increase in the $I_{\text{D3}}/I_{\text{All}}$ ratio of C-ZSBC after adding kaolin can be attributed to the intensification of aromatic interlayer gap defects, which leads to an increase in active sites and better gasification performance.⁴³

The Raman analysis confirms that the addition of kaolin weakens the promotion of pyrolysis on the graphitization degree of char. This reduction in the graphitization degree has a positive impact on increasing the amorphous carbon structure and defects in the carbon crystal of char. These findings further support the notion that adding kaolin increases the degree of disorder of char, ultimately improving its gasification activity.

3.4.4. SEM Analysis. Figure 7 displays the surface microstructures of C-ZSBC and C-ZSBC-K. Figure 7a shows the surface of C-ZSBC. It appears smooth with a dense and regular structure, and its pore structure is almost invisible. Figure 7b illustrates the granular carbon structure on the C-ZSBC-K

surface. It appears to be loose and exhibits a large number of pores. Combined with the results of XRD and Raman, it can be comprehensively concluded that after adding kaolin, the initially disordered graphite structure in C-ZSBC becomes even more disordered, thus increasing the number of defects in microcrystals. This may explain the rich pore structure observed in C-ZSBC-K. The presence of a rich pore structure is conducive to the entry of the gasification agent into the coal char particles, enabling its participation in the gasification process. This ultimately results in a better gasification performance.

3.4.5. XPS Analysis. Figure 8 shows the XPS spectra and fitting peaks of C and O elements of C-ZSBC and C-ZSBC-K. The surface carbon atom contents of C-ZSBC and C-ZSBC-K are 86.24% and 86.46% respectively. C 1s of C-ZSBC and C-ZSBC-K includes >C-C< (284.6 eV), >C-H (284.6 eV), >C-O- (285.4 eV), >C=O (286.6 eV), and -COOH (289.1 eV) structures.⁴⁴ The structural contents of C-C/C-H, >C-O-, >C=O, and -COOH in C-ZSBC are 65.84%, 19.11%, 11.27% and 3.78% respectively. The addition of kaolin leads to a decrease in the content of the C-C/C-H structure in C-ZSBC, indicating a reduction in its graphitization degree.¹² Compared with C-ZSBC-K, the content of >C-O-, >C=O, -COOH structures in C-ZSBC-K has increased, which is because C-ZSBC-K has a porous structure to adsorb certain oxygen and water molecules, which oxidizes the carbon layer skeleton and supplements the oxygen-containing structure removed during pyrolysis. After adding kaolin, the reduction of graphitization degree of C-ZSBC and the increase of >C-O-, >C=O, and -COOH structures are conducive to the gasification.²¹

The surface oxygen atom contents of C-ZSBC and C-ZSBC-K are 10.5% and 11.22%, respectively. The O 1s spectra of C-ZSBC and C-ZSBC-K include >C=O (530.7 eV), >C-O- (532.5 eV) and COO- (534.0 eV) structures (Table 8).⁴⁵ In C-ZSBC, the contents of >C=O, >C-O-, and COO- structures are 35.31%, 37.22%, and 27.47%, respectively. Upon adding kaolin, there is an increase in the >C=O structure within C-ZSBC, causing an increase in oxygen-containing functional groups, which in turn improves the gasification performance of the material.⁴⁶ Additionally, oxygen-containing functional groups enhance the anisotropy of char and increase the proportion of amorphous and defective carbon structures. Consequently, the char's pore structure becomes more abundant, leading to improved gasification performance.

4. CONCLUSION

This study investigated the effects of adding kaolin on ZSBC and ZSBC-K. Analysis of the TG and DTG curves obtained during sample pyrolysis, combustion, and gasification showed that the addition of kaolin reduced the combustion and pyrolysis reactivity of ZSBC. This reduction occurred due to kaolin's ability to adsorb the catalytic alkali metal present in ZSBC, thereby decreasing its reaction activity. After the addition of kaolin, the gasification activity of ZSBC showed a significant improvement. The gasified samples of ZSBC and ZSBC-K were subjected to characterization and analysis, with a study conducted on the effect of kaolin addition on the structure of coal char. The results indicated that the addition of kaolin weakened the promotion of pyrolysis on the graphitization degree of char. This weakening of the graphitization degree had a positive impact on increasing the amorphous carbon structure and defective carbon crystal in

char, thereby enhancing the disorder degree of char and forming char pores. This, in turn, led to a further improvement in gasification activity. In addition, the presence of oxygen-containing structures and defect sites in coal char facilitated the cracking and gasification of macromolecular polymer aromatic structures.

AUTHOR INFORMATION

Corresponding Author

Wenlong Mo – State Key Laboratory of Chemistry and Utilization of Carbon-Based Energy Resources and Key Laboratory of Coal Clean Conversion & Chemical Engineering Process (Xinjiang Uyghur Autonomous Region), School of Chemical Engineering and Technology, Xinjiang University, Urumqi 830046 Xinjiang, People's Republic of China; orcid.org/0000-0003-3837-0915; Email: mowenlong@xju.edu.cn

Authors

Nan Xiao – State Key Laboratory of Chemistry and Utilization of Carbon-Based Energy Resources and Key Laboratory of Coal Clean Conversion & Chemical Engineering Process (Xinjiang Uyghur Autonomous Region), School of Chemical Engineering and Technology, Xinjiang University, Urumqi 830046 Xinjiang, People's Republic of China; orcid.org/0009-0007-4886-8131

Xiaobo Hu – State Key Laboratory of Chemistry and Utilization of Carbon-Based Energy Resources and Key Laboratory of Coal Clean Conversion & Chemical Engineering Process (Xinjiang Uyghur Autonomous Region), School of Chemical Engineering and Technology, Xinjiang University, Urumqi 830046 Xinjiang, People's Republic of China

Guanjun Jing – State Key Laboratory of Chemistry and Utilization of Carbon-Based Energy Resources and Key Laboratory of Coal Clean Conversion & Chemical Engineering Process (Xinjiang Uyghur Autonomous Region), School of Chemical Engineering and Technology, Xinjiang University, Urumqi 830046 Xinjiang, People's Republic of China

Xing Fan – State Key Laboratory of Chemistry and Utilization of Carbon-Based Energy Resources and Key Laboratory of Coal Clean Conversion & Chemical Engineering Process (Xinjiang Uyghur Autonomous Region), School of Chemical Engineering and Technology, Xinjiang University, Urumqi 830046 Xinjiang, People's Republic of China; Key Laboratory of Chemistry and Chemical Engineering on Heavy Carbon Resources of Yili Kazakh Autonomous Prefecture, Yili Normal University, Yining 835000 Xinjiang, People's Republic of China; College of Chemical and Biological Engineering, Shandong University of Science and Technology, Qingdao 266590 Shandong, People's Republic of China

Xiaoqin Yang – Xinjiang Yihua Chemical Industry Co, Ltd, Changji 831700, People's Republic of China

Shupeizhang – Xinjiang Yihua Chemical Industry Co, Ltd, Changji 831700, People's Republic of China

Xianyong Wei – State Key Laboratory of Chemistry and Utilization of Carbon-Based Energy Resources and Key Laboratory of Coal Clean Conversion & Chemical Engineering Process (Xinjiang Uyghur Autonomous Region), School of Chemical Engineering and Technology, Xinjiang University, Urumqi 830046 Xinjiang, People's Republic of

China; Key Laboratory of Coal Processing and Efficient Utilization, Ministry of Education, China University of Mining and Technology, Xuzhou 221116 Jiangsu, People's Republic of China; orcid.org/0000-0001-7106-4624

Complete contact information is available at:
<https://pubs.acs.org/10.1021/acsomega.3c02101>

Notes

The authors declare no competing financial interest.

ACKNOWLEDGMENTS

The project was supported by the High Quality Development Special Project for Science and Technology Supporting Industry from Changji prefecture, Xinjiang, China (2022Z04) "Research, Development and Application of Key Technologies for Improving Quality and Efficiency in Coal Chemical Industry", a special project from the State Key Laboratory of Chemistry and Utilization of Carbon-based Energy Resources "Element migration and transformation mechanism and reactor simulation and optimization of fluidized bed gasifier based on Zhundong coal", and the Natural Science Foundation of Shandong Province (ZR2021MB115).

REFERENCES

- (1) Liu, K.; Wei, B.; Zhang, Y.; Wang, J.; Chen, L.; Wu, W.; Tan, H.; Yao, H. Fe Occurrence Form and Slagging Mechanism on Water-Wall during High Iron Zhundong Coal Combustion Process. *Fuel* **2022**, *315*, 123268.
- (2) Yang, H.; Jin, J.; Liu, D.; Wang, Y.; Zhao, B. The Influence of Vermiculite on the Ash Deposition Formation Process of Zhundong Coal. *Fuel* **2018**, *230*, 89–97.
- (3) Huang, Q.; Zhang, Y.; Yao, Q.; Li, S. Mineral Manipulation of Zhundong Lignite towards Fouling Mitigation in a Down-Fired Combustor. *Fuel* **2018**, *232*, 519–529.
- (4) Yu, Z.; Jin, J.; Hou, F.; Zhang, Y.; Wang, G.; Liu, B.; Zhai, Z. Understanding Effect of Phosphorus-Based Additive on Ash Deposition Characteristics during High-Sodium and High-Calcium Zhundong Coal Combustion in Drop-Tube Furnace. *Fuel* **2021**, *287*, 119462.
- (5) Zhu, C.; Tu, H.; Bai, Y.; Ma, D.; Zhao, Y. Evaluation of Slagging and Fouling Characteristics during Zhundong Coal Co-Firing with a Si/Al Dominated Low Rank Coal. *Fuel* **2019**, *254*, 115730.
- (6) Zhang, X.; Liu, H.; Xing, H.; Wang, G.; Deng, H.; Hu, H.; Li, X.; Yao, H. Correlations between the Sodium Adsorption Capacity and the Thermal Behavior of Modified Kaolinite during the Combustion of Zhundong Coal. *Fuel* **2019**, *237*, 170–177.
- (7) Wornat, M. J.; Nelson, P. F. Effects of Ion-Exchanged Calcium on Brown Coal Tar Composition as Determined by Fourier Transform Infrared Spectroscopy. *Energy Fuels* **1992**, *6* (2), 136–142.
- (8) Shibaoka, M.; Ohtsuka, Y.; Wornat, M. J.; Thomas, C. G.; Bennett, A. J. R. Application of Microscopy to the Investigation of Brown Coal Pyrolysis. *Fuel* **1995**, *74*, 1648–1653.
- (9) Xu, S. Q.; Zhou, Z. J.; Xiong, J.; Yu, G. S.; Wang, F. Effects of Alkaline Metal on Coal Gasification at Pyrolysis and Gasification Phases. *Fuel* **2011**, *90* (5), 1723–1730.
- (10) Casanova, R.; Cabrera, A. L.; Heinemann, H.; Somorjai, G. A. Calcium Oxide and Potassium Hydroxide Catalysed Low Temperature Methane Production from Graphite and Water Comparison of Catalytic Mechanisms. *Fuel* **1983**, *62* (10), 1138–1144.
- (11) Pereira, P.; Somorjai, G. A.; Heinemann, H. Catalytic Steam Gasification of Coals. *Energy Fuels* **1992**, *6* (4), 407–410.
- (12) Wang, N.; Mao, M.; Mao, G.; Yin, J.; He, R.; Zhou, H.; Li, N.; Liu, Q.; Zhi, K. Investigation on Carbide Slag Catalytic Effect of Mongolian Bituminous Coal Steam Gasification Process. *Chemosphere* **2021**, *264*, 128500.
- (13) Zhao, Y.; Liu, L.; Qiu, P. H.; Xie, X.; Chen, X. Y.; Lin, D.; Sun, S. Z. Impacts of Chemical Fractionation on Zhundong Coal's Chemical Structure and Pyrolysis Reactivity. *Fuel Process. Technol.* **2017**, *155*, 144–152.
- (14) Liu, Q.; Wang, S.; Zheng, Y.; Luo, Z.; Cen, K. Mechanism Study of Wood Lignin Pyrolysis by Using TG-FTIR Analysis. *Journal of Analytical and Applied Pyrolysis* **2008**, *82* (1), 170–177.
- (15) Qiu, P. H.; Zhao, Y.; Chen, X. Y.; Xu, J. J.; Du, Y. W.; Fang, L. X.; Sun, S. Z.; et al. Effects of Alkali and Alkaline Earth Metallic Species on Pyrolysis Characteristics and Kinetics of Zhundong Coal. *Journal of Fuel Chemistry and Technology* **2014**, *10*, 1178–1189.
- (16) Shi, Q.; Qin, B.; Bi, Q.; Qu, B. An Experimental Study on the Effect of Igneous Intrusions on Chemical Structure and Combustion Characteristics of Coal in Daxing Mine, China. *Fuel* **2018**, *226*, 307–315.
- (17) Wu, Z.; Wang, S.; Zhao, J.; Chen, L.; Meng, H. Thermal Behavior and Char Structure Evolution of Bituminous Coal Blends with Edible Fungi Residue during Co-Pyrolysis. *Energy Fuels* **2014**, *28* (3), 1792–1801.
- (18) Zhao, Z.; Li, W.; Qiu, J.; Wang, X.; Li, B. Influence of Na and Ca on the Emission of NO_x during Coal Combustion. *Fuel* **2006**, *85* (5–6), 601–606.
- (19) Hu, Y.; Wang, Z.; Cheng, X.; Liu, M.; Ma, C. Effects of Catalysts on Combustion Characteristics and Kinetics of Coal-Char Blends. *IOP Conf. Ser.: Earth Environ. Sci.* **2018**, *133*, 012023.
- (20) Wu, L.; Qiao, Y.; Gui, B.; Wang, C.; Xu, J.; Yao, H.; Xu, M. Effects of Chemical Forms of Alkali and Alkaline Earth Metallic Species on the Char Ignition Temperature of a Loy Yang Coal under O₂/N₂ Atmosphere. *Energy Fuels* **2012**, *26* (1), 112–117.
- (21) Lu, Y.; Wang, Y.; Zhang, J.; Xu, Y.; Li, G.; Zhang, Y. Investigation on the Catalytic Effect of AAEMs in Zhundong Coal on the Combustion Characteristics of Changji Oil Shale and Its Kinetics. *Energy* **2019**, *178*, 89–100.
- (22) Ren, J.; Xie, C.; Guo, X.; Qin, Z.; Lin, J. Y.; Li, Z. Combustion Characteristics of Coal Gangue under an Atmosphere of Coal Mine Methane. *Energy Fuels* **2014**, *28* (6), 3688–3695.
- (23) Mo, W.; Wu, Z.; He, X.; Qiang, W.; Wei, B.; Wei, X.; Wu, Y.; Fan, X.; Ma, F. Functional Group Characteristics and Pyrolysis/Combustion Performance of Fly Ashes from Karamay Oily Sludge Based on FT-IR and TG-DTG Analyses. *Fuel* **2021**, *296*, 120669.
- (24) Hu, X.; Yang, X.; Mo, W.; Zhang, S.; Ji, G.; Wei, X.; Fan, X. Structural characteristics and thermal conversion performance of ash and slag from circulating fluidized bed gasifier. *Journal of Fuel Chemistry and Technology* **2022**, *50* (10), 1361–1371.
- (25) Carrazza, J.; Tysoe, W. T.; Heinemann, H.; Somorjai, G. A. Gasification of Graphite with Steam below 900 K Catalyzed by a Mixture of Potassium Hydroxide and Transition Metal Oxide. *J. Catal.* **1985**, *96* (1), 234–241.
- (26) Pereira, P.; Csencsits, R.; Somorjai, G. A.; Heinemann, H. Steam Gasification of Graphite and Chars at Temperatures < 1000 K over Potassium-Calcium-Oxide Catalysts. *J. Catal.* **1990**, *123* (2), 463–476.
- (27) Miao, Z.; Guo, F.; Zhao, X.; Guo, Z.; Guo, Y.; Zhang, Y.; Wu, J. Effects of Acid Treatment on Physicochemical Properties and Gasification Reactivity of Fine Slag from Texaco Gasifier. *Chem. Eng. Res. Des.* **2021**, *169*, 1–8.
- (28) Ginter, D. M.; Somorjai, G. A.; Heinemann, H. Factors Affecting the Reactivity of Chars and Cokes during Low-Temperature (640 °C) Steam Gasification. *Energy Fuels* **1993**, *7*, 393–398.
- (29) Feng, Z. H.; Liu, L.; Mo, W. L.; Wei, X. Y.; Yuan, J. R.; Fan, X.; Guo, W. C.; Guo, J.; Niu, J. M. Copyrolysis and Cocombustion Performance of Karamay Oily Sludge and Zhundong Subbituminous Coal. *ACS Omega* **2022**, *7* (48), 43793–43802.
- (30) Yin, Y.; Yin, J.; Zhang, W.; Tian, H.; Hu, Z.; Ruan, M.; Xu, H.; Liu, L.; Yan, X.; Chen, D. FT-IR and Micro-Raman Spectroscopic Characterization of Minerals in High-Calcium Coal Ashes. *Journal of the Energy Institute* **2018**, *91* (3), 389–396.
- (31) Liang, D.; Xie, Q.; Wan, C.; Li, G.; Cao, J. Evolution of Structural and Surface Chemistry during Pyrolysis of Zhundong Coal

in an Entrained-Flow Bed Reactor. *Journal of Analytical and Applied Pyrolysis* **2019**, *140*, 331–338.

(32) Diao, R.; Zhu, X.; Wang, C.; Zhu, X. Synergistic Effect of Physicochemical Properties and Reaction Temperature on Gasification Reactivity of Walnut Shell Chars. *Energy Conversion and Management* **2020**, *204*, 112313.

(33) Li, M.; Zhang, Z.; Wu, X.; Fan, J. Experiment and Mechanism Study on the Effect of Kaolin on Melting Characteristics of Zhundong Coal Ash. *Energy Fuels* **2016**, *30* (9), 7763–7769.

(34) Ayiania, M.; Smith, M.; Hensley, A. J. R.; Scudiero, L.; McEwen, J. S.; Garcia, P. M. Deconvoluting the XPS Spectra for Nitrogen-Doped Chars: An Analysis from First Principles. *Carbon* **2020**, *162*, 528–544.

(35) Yaseri, S.; Masoomi Verki, V.; Mahdikhani, M. Utilization of High Volume Cement Kiln Dust and Rice Husk Ash in the Production of Sustainable Geopolymer. *Journal of Cleaner Production* **2019**, *230*, 592–602.

(36) Li, W.; Shen, Y.; Guo, J.; Kong, J.; Wang, M.; Chang, L. Effects of Additives on Coke Reactivity and Sulfur Transformation during Co-Pyrolysis of Long Flame Coal and High-Sulfur Coking Coal. *ACS Omega* **2021**, *6* (50), 34967–34976.

(37) Sonibare, O. O.; Haeger, T.; Foley, S. F. Structural Characterization of Nigerian Coals by X-Ray Diffraction, Raman and FTIR Spectroscopy. *Energy* **2010**, *35* (12), 5347–5353.

(38) Diao, R.; Wang, C.; Zhu, X. F. Influence of Carbonization Degree of Walnut Shell Char on Pore Structure and Combustion Characteristics. *Journal of Fuel Chemistry and Technology* **2019**, *10*, 1146–1180.

(39) Burket, C. L.; Rajagopalan, R.; Foley, H. C. Overcoming the Barrier to Graphitization in a Polymer-Derived Nanoporous Carbon. *Carbon* **2008**, *46* (3), 501–510.

(40) Huang, S.; Wu, S.; Wu, Y.; Gao, J. Structure Characteristics and Gasification Activity of Residual Carbon from Updraft Fixed-Bed Biomass Gasification Ash. *Energy Conversion and Management* **2017**, *136*, 108–118.

(41) Zhang, X.; Song, X.; Su, W.; Wei, J.; Bai, Y.; Yu, G. In-Situ Study on Gasification Reaction Characteristics of Ningdong Coal Chars with CO₂. *Journal of Fuel Chemistry and Technology* **2019**, *47* (4), 385–392.

(42) Sheng, C. Char Structure Characterised by Raman Spectroscopy and Its Correlations with Combustion Reactivity. *Fuel* **2007**, *86* (15), 2316–2324.

(43) Zaida, A.; Bar, Z. E.; Radovic, L. R.; Lee, Y. J. Further Development of Raman Microprobe Spectroscopy for Characterization of Char Reactivity. *Proceedings of the Combustion Institute* **2007**, *31* (2), 1881–1887.

(44) Niu, C.; Xia, W.; Xie, G. Effect of Low-Temperature Pyrolysis on Surface Properties of Sub-Bituminous Coal Sample and Its Relationship to Flotation Response. *Fuel* **2017**, *208*, 469–475.

(45) Pietrzak, R.; Grzybek, T.; Wachowska, H. XPS Study of Pyrite-Free Coals Subjected to Different Oxidizing Agents. *Fuel* **2007**, *86* (16), 2616–2624.

(46) Zhao, D.; Liu, H.; Zhu, D.; Qin, M. Effect of O-Containing Functional Groups Produced by Preoxidation on Zhundong Coal Gasification. *Fuel Process. Technol.* **2020**, *206*, 106480.